1 2 3 4 Unique growth and morphology properties of Clade 5 Clostridioides difficile strains 5 revealed by single-cell time-lapse microscopy 6 7 John W. Ribis<sup>1,2\*‡</sup>, César Nieto<sup>3\*</sup>, Nicholas V. DiBenedetto<sup>1,2</sup>, Anchal Mehra, Pola Kuhn<sup>1,2</sup>, 8 Qiwen Dong<sup>1</sup>, Irene Nagawa, Imane El Meouche, Bree B. Aldridge, Mary J. Dunlop, Rita 9 Tamayo, <sup>4</sup> Abhyudai Singh, <sup>3</sup> Aimee Shen<sup>1†</sup> 10 11 12 13 **Affiliations** 14 <sup>1</sup>Department of Molecular Biology and Microbiology, Tufts University School of Medicine, Boston, Massachusetts, USA, <sup>2</sup> Graduate School of Biomedical Sciences, Tufts University 15 16 School of Medicine, Boston, Massachusetts, USA. <sup>3</sup>Department of Electrical and Computer Engineering, University of Delaware, Newark, DE 19716, USA. <sup>4</sup>Department of Microbiology 17 18 and Immunology, University of North Carolina at Chapel Hill School of Medicine, Chapel Hill, NC, USA, <sup>5</sup>INSERM, Université Paris Cité, Université Sorbonne Paris Nord, Inserm, IAME, F-19 75018, Paris, France, <sup>6</sup>Department of Biomedical Engineering, Tufts University School of 20 Engineering, Medford, Massachusetts, USA, <sup>7</sup>Biomedical Engineering, Boston University, 21 22 Boston, MA 02215. 23 \*These authors contributed equally to this work. 24 <sup>‡</sup>Current address: Nikon Instruments 25 26 <sup>†</sup>Address correspondence to Aimee Shen, aimee.shen@tufts.edu 27 28 Phone number: (617)636-3792

**Abstract** 

Clostridioides difficile is a gastrointestinal pathogen of both humans and agricultural animals and thus a major One Health threat. The *C. difficile* species consists of five main clades, with Clade 5 currently undergoing speciation from Clades 1-4. Clade 5 strains are highly prevalent in agricultural animals and can cause zoonotic infections, suggesting that these strains have evolved phenotypes that distinguish them from Clade 1-4 strains. Here, we compare the growth properties of Clade 5 strains to those of Clade 1-4 strains using anaerobic time-lapse microscopy coupled with automated image analysis. Our analyses indicate that Clade 5 strains grow faster and are more likely to form long chains of cells than Clade 1-4 strains. Using comparative genomic and CRISPRi analyses, we show that the chaining phenotype of Clade 5 strains is driven by the orientation of the invertible *cmr* switch sequence, with chaining strains exhibiting a bias to the *cmr*-ON state. Interestingly, Clade 5 strains with a bias towards the *cmr*-ON state shifted to a largely *cmr*-OFF state during murine infection, suggesting that the *cmr*-OFF state is under positive selection during infection. Collectively, our data reveal that Clade 5 strains have distinct growth properties, which may allow them to inhabit diverse ecological niches.

# **Author Summary**

The Clade 5 strains of the *Clostridioides difficile* species are so phylogenetically divergent that they almost meet the threshold of being a distinct species. Although these strains are ubiquitously isolated from agricultural and environmental settings and an important source of zoonotic and community-acquired infections, it is unclear whether they have distinct phenotypic properties that allow them to colonize diverse hosts or persist in the environment. By combining a novel anaerobic time-lapse microscopy method with automated image analysis, we discovered that Clade 5 strains grow faster than strains from other *C. difficile* clades and that they frequently form long chains. These chaining properties are driven by the environmentally responsive expression of a non-canonical signal transduction system, which our analyses suggest is selected against during murine infection. Collectively, our analyses reveal that Clade 5 strains have distinct growth properties that may promote their persistence in the environment.

#### Introduction

59

60

61

62

63

64

65

66

67

68

69

70

71

72

73

74

75

76

77

78

79

80

81

82

83

84

85

86

87

88

89

Clostridioides difficile is a leading cause of nosocomial infections in the United States, with approximately 500,000 new infections and 14,000 deaths being attributed to this organism annually [1, 2]. As an obligate anaerobe, C. difficile relies on its hardy, metabolically dormant spore form to survive outside the host and transmit disease to new hosts [3]. When C. difficile spores are ingested by susceptible hosts [4, 5], they germinate and outgrow into vegetative cells that subsequently colonize the colon. The vegetative cells secrete toxins that damage gut epithelial tissue [6], which triggers an inflammatory response that can cause disease pathologies ranging from mild diarrhea to pseudomembranous colitis and even death [2, 4]. C. difficile also causes recurrent infections in ~20% of infections, which can lead to more severe disease symptoms [2, 7, 8]. C. difficile's success as a pathogen may be related to its tremendous genetic diversity [9-11], with genomic analyses indicating that C. difficile's core genome represents only ~10-20% of its pan-genome [9, 10]. The plasticity of its "open" pan-genome likely helps C. difficile colonize the gastrointestinal tract of diverse animals, from mammals to invertebrates, and persist in environmental reservoirs like sewage and compost [12]. Indeed, the C. difficile species is so genetically diverse that it has been divided into five distinct phylogenetic clades based on multi-locus sequence typing (MLST) analyses, and the clades have been further subdivided into different ribotypes (RTs) or sequence types (STs) [10, 13]. Between these five clades, there are notable differences in geographic and host distributions. Clade 1 is the largest, most heterogeneous clade with the broadest geographic distribution [14, 15]. It includes over 200 STs, which can contain both toxin-producing and nontoxigenic strains, including the well-characterized, genetically tractable toxigenic strain 630 [9]. Clade 2 harbors epidemic-associated strains found within the ribotype 027 (RT027) lineage. Strains from this ribotype have been associated with outbreaks in hospitals, particularly in North America, due to their frequent resistance to fluoroquinolones [16-18]. These epidemic strains can also cause severe disease symptoms in part due to their production of three toxins: TcdA, TcdB, and CDT (binary toxin) [6]. Although RT027 strains have frequently been associated with "hypervirulence," there is considerable phenotypic diversity within this lineage with respect to virulence, toxin production levels, flagellar motility, and sporulation [19-22].

91

92

93

94

95

96

97

98

99

100

101

102

103

104

105

106

107

108

109

110

111

112

113

114

115

116

117

118

119

120

Clade 3 strains are relatively uncommon and harbor a unique cell surface due to their lack of CwpV production [23], but phenotypic analyses of biofilm formation and motility suggest that they share similarities with Clade 2 strains like R20291 [24]. Clade 4 contains RT017 (ST37) strains that only encode a single toxin, TcdB (i.e., TcdA-CDT-), and are often clindamycin- and fluoroguinolone-resistant. RT017 strains have been associated with outbreaks in Europe and North America and are the most common strains found in Asia [25]. Clade 5 is the most genetically distant from the other 4 main C. difficile clades and is thought to have emerged before Clades 1-4 [26]. While the average nucleotide identity (ANI) for Clades 1-4 ranges between 97.1 - 99.8%, Clade 5 strains exhibit ANI values around 96%, which is close to the ANI value demarcation used by NCBI to define organisms of the same species [10, 27]. Thus, Clade 5 strains appear to be actively diverging from Clades 1-4 [10]. Clade 5 strains are an increasing problem in healthcare and agricultural settings because they can cause severe disease in humans and are commonly found in livestock, particularly pigs [12, 28]. While other C. difficile strains have been known to infect both humans and animals, only Clade 5 strains have been associated with zoonotic transmission from both animal-tohuman and human-to-animal [28, 29]. The mechanisms underlying this bidirectional zoonotic transmission are poorly understood, but the increased carriage of antimicrobial resistance genes by Clade 5 strains may contribute to their ability to persist in agricultural and community settings [28, 30]. Thus, Clade 5 strains are of particular relevance from a One Health perspective [12, 31], especially since they frequently cause community-acquired infections [30] and are often detected in retail foods [32]. These observations highlight the importance of understanding the unique properties of this group of strains. Indeed, a recent genomic analysis suggests that RT078/ST11 strains within Clade 5 frequently carry zinc acquisition and homeostasis genes [11]. Despite numerous genomic analyses revealing the remarkable genetic diversity of C. difficile strains, relatively few studies have investigated the phenotypic diversity between strains from different clades. Clade-specific differences in colony morphology between Clade 5 strains relative to Clade 1-4 strains have been described in a limited set of analyses [26, 33], suggesting that differences in growth and/or cellular morphology may exist within clades. While differences in bulk growth rates between C. difficile strains have been reported [34], most phenotypic analyses have been conducted on a limited subset of strains within a given clade.

Furthermore, systematic comparisons of the growth properties of different clades have only recently been described [35], while comparisons of their cell morphology have not been performed to date.

Here, we compare the growth properties of multiple strains derived from all five phylogenetic clades of *C. difficile* using anaerobic time-lapse microscopy. These analyses unexpectedly reveal striking differences in the growth and cell morphology of the Clade 5 lineage relative to strains from Clades 1-4. Specifically, we found that Clade 5 strains grow faster and frequently form long chains, in contrast with strains from Clade 1-4 strains. Genomic comparisons and genetic analyses indicate that the chaining phenotype of Clade 5 strains is driven by the phase-variable expression of the *cmrRST* operon by the invertible *cmr* switch [33]. Interestingly, we found that Clade 5 strains with a strong *cmr*-ON bias mostly reverted to a *cmr*-OFF phenotype during murine infection. Taken together, our data reveal that Clade 5 strains have unique growth properties relative to Clade 1-4 strains that may contribute to the widespread distribution of Clade 5 strain among diverse animal hosts.

# **Results**

# Development of a simple method for time-lapse imaging under anaerobic conditions

Time-lapse imaging of single cells has been widely used to study phenotypic heterogeneity in bacteria, which can impact important traits like antibiotic resistance and virulence [33, 36-39]. However, live single-cell analyses in *C. difficile* have been complicated by its inability to grow in the presence of atmospheric oxygen [40]. While time-lapse microscopy analyses of *C. difficile* have previously been reported, they require custom growth chambers to maintain anaerobic conditions [41] and thus may limit the accessibility of these experimental systems to a broad range of investigators.

To overcome these limitations, we established a simple system that relies solely upon commercially available reagents and materials to grow *C. difficile* cells under anaerobic conditions. This system uses gas-tight, adhesive Gene Frames, which have been used extensively in imaging applications for bacteria [42]. Notably, the gas-impermeability of these commercial seals allows anaerobic conditions to be maintained when agarose pads made with growth media

are prepared in the anaerobic chamber (**Figure 1**). Gene Frames also generate thick agarose pads, which are critical for *C. difficile* to grow in a sealed system under ambient conditions. After agarose pads are prepared in the anaerobic chamber, *C. difficile* cultures are inoculated onto the pads, and the pads are sealed with a coverslip. The growth chamber is then removed from the chamber and imaged on a heated microscope stage under ambient conditions for up to 6 hours or until *C. difficile* stops growing as a monolayer.

# Time-lapse microscopy reveals clade-specific differences in elongation rate and cell length

Having established an anaerobic time-lapse imaging setup, we compared the single-cell growth properties of representative *C. difficile* strains from Clade 1 (630, ribotype (RT) 012), Clade 2 (R20291, RT027), Clade 3 (E15, RT075), Clade 4 (M68, RT017), and Clade 5 (M120, RT078) (**Figure 2, Table 1**). The five "representative" strains were all isolated from patients with *C. difficile*-associated disease and are frequently used as reference genomes for their clades and ribotype groups. Notably, RT027 (ST1), RT017 (ST45), and RT078 (ST11) strains are from ribotypes/ multi-locus sequencing types that are frequently isolated from patients with *C. difficile* infection (CDI) [12, 16, 19, 25]. In contrast, Clade 3 strains are more rare and the least characterized of *C. difficile* strains [23].

The growth properties of single cells visualized by time-lapse microscopy were quantified using Deep Learning for Time-lapse Analysis (DeLTA) software, which rapidly and accurately segments and tracks bacteria growing in two dimensions on agarose pads [43, 44]. This software uses deep convolutional neural networks to analyze time-lapse microscopy images, allowing the growth properties of individual cells growing in microcolonies on agarose pads to be determined. The segmentation and tracking of *C. difficile* cells were highly accurate (**Figure 1**), and minimal user input or post-image processing was needed to obtain growth property measurements.

Robust growth was observed for all strains using our system. Growth was quantified by measuring the elongation rate, which was defined as doublings/hr to indicate the number of times that a cell's length doubles in one hour. The elongation rate (doublings/hr) is distinct from the doubling time, or generation time, which represents the length of *time* that it takes before a bacterium divides. Instead, the elongation rate reflects how fast the cell is increasing in length

184

185

186

187

188

189

190

191

192

193

194

195

196

197

198

199

200

201

202

203

204

205

206

207

208

209

210

211

212

213

over time. Notably, the Clade 5 strain M120 elongated the fastest (2.1 doublings/hr, p < 0.05), followed by Clade 3 E15 (2.0 doublings/hr) and Clade 2 strain R20291 (1.8 doublings/hr), and then Clade 1 strain 630 and Clade 4 strain M68 (1.6-1.7 doublings/hr) (**Figure 2A**). Importantly, the differences in single-cell elongation rates measured for the five strains were also observed in bulk population analyses of their growth using optical density in TYC and BHIS media (Figure 2B & S1). These analyses confirmed that the Clade 5 strain M120 grew faster (based on optical density-based analyses) in these media than the Clade 1-4 strains (p < 0.001). In contrast, negligible differences in bulk growth rates were observed between Clade 1-4 strains in BHIS media, although, in TYC medium, the Clade 3 strain grew faster than Clades 1, 2, and 4 strains (**Figures 2B & S1**). The Clade 5 strain M120 exhibited another distinct growth property from the Clade 1-4 strains. While strains from Clades 1-4 produced cells of similar length prior to cell division, with an average apparent length of ~13 µm, cells of Clade 5 strain M120 were significantly longer, with an average apparent length of ~22 µm. Indeed, cells ~50 µm were readily observed for the Clade 5 strain M120 (**Figure 2C**), and these cells appeared to bend readily (**Figure 2D**). By incorporating the FM4-64 membrane stain into the agarose pads to visualize division septa [45], we assessed whether the Clade 5 strain M120 forms chains vs. filaments, These analyses revealed that septa were readily observed in Clade 5 strain M120 across the length of a given cell (**Figure 3, inset**), Since the spacing between division septa was relatively consistent, the Clade 5 strain M120 appear to undergo cell separation less efficiently than strains from the other clades tested. Indeed, cell separation in strain M120 was so inefficient that it was often necessary to stitch together several fields of view to fully visualize M120 chains, which approached several hundred microns and even up to ~1 mm in length (Figure 3). Clade 5 clinical isolates typically form long chains and grow more quickly than strains from other clades Since prior work indicated that Clade 5 strains produce colony morphologies distinct from Clade 1, 2, and 4 strains [26], we sought to determine whether the striking cell chaining phenotype and faster growth rate observed in Clade 5 strain M120 were properties shared by

other Clade 5 strains. Thus, we compared the single-cell growth properties of five additional

215

216

217

218

219

220

221

222

223

224

225

226

227

228

229

230

231

232

233

234

235

236

237

238

239

240

241

242

243

244

Clade 5 clinical isolates obtained from several hospitals around the country on TYC agarose (**Table 1**) using time-lapse microscopy analyses (**Figure 2**). Clade 1 strain 630 was included as a control since it does not form chains in any of the conditions we have tested. These analyses revealed that all but one of the Clade 5 strains tested formed long chains, with TAL29600 forming the longest chains (29 µm on average, Figure 4A-C). In contrast, strain TAL29996 formed shorter chains that were comparable in length to those observed for strains from Clades 1-4 (12-13 µm, **Figures 2B & 4C**). Notably, DeLTA segmented many Clade 5 chains as single cells because cell separation (i.e., invagination) had not yet initiated at division septa visualized via FM4-64 staining. To overcome this limitation and accurately quantify cell length within long chains, namely the distance between division septa, we modified our image processing pipeline to use a thresholding method to detect division septa. After generating masks in DeLTA to segment the chains, we modified the mask so that only the interior of the contour was analyzed. We then applied an adaptive thresholding method to identify division septa based on their elevated fluorescence relative to the long axis of the cell; the thresholds were defined using a Gaussian-weighted method (Figure 4A, red dots, Figure **4B**). Septa detected with this automated method were also manually inspected. These analyses revealed that the average length of cells within the chains of cells made by Clade 5 strains is only slightly longer than the average length of cells made by strains that do not form chains, namely Clade 1 strain 630 and Clade 5 strain TAL29996 (Figure 4C, Table 2). For example, the Clade 5 strains that produced "he l'ngest chains (TAL29600 and TAL30550) had average cell lengths of 14 and 12 µm, respectively, which is only 30-50% longer than the non-chaining strains 630 (Clade 1, 8.5 µm) and TAL29996 (Clade 5, 9.4 µm) (**Table 2**). Notably, even though the Clade 5 strain TAL29996 did not form chains, it still exhibited higher elongation rates, which were similar to those measured for other Clade 5 strains (2.1 doublings/hr vs. 1.7 doublings/hr for Clade 1 strain 630, Figure 4D). Importantly, the additional Clade 5 strains tested also grew faster in bulk optical densitybased analyses in broth culture than Clade 1-4 strains irrespective of their ability to form chains (Figure S2). To assess whether these findings would extend to additional Clade 5 strains vs. Clade 1-4 strains, we analyzed the growth of additional strains from all five clades in broth culture. These analyses confirmed that Clade 1-4 strains grow at similar rates in BHIS media, which are slower than those observed for the nine Clade 5 strains analyzed in this media

(**Figure S2**). However, Clade 3 strains grew relatively faster than the Clade 1 630 strain in TYC medium, but their growth was still slower than the Clade 5 strain M120 (**Figure S2**). Taken together, these analyses strongly suggest that Clade 5 strains grow faster than Clade 1-4 strains and are more likely to form chains, presumably because their cell separation mechanisms are less efficient.

#### Cell chaining in Clade 5 strains is not dependent on growth on a solid medium.

C. difficile has previously been shown to promote cell elongation and chain formation upon induction of the *cmrRST* locus [33], which encodes a non-canonical signal transduction system. Expression of this locus is also responsive to c-di-GMP levels [46], which increases in cells grown on solid surfaces such as in a biofilm or on an agar plate [46]. To test whether the chaining phenotype observed in Clade 5 strains is induced by growth on a surface, we assessed the chaining properties of Clade 5 strains during logarithmic growth in rich medium broth culture using the fluorescent D-amino acid label, HADA, to stain septa. These analyses revealed that Clade 5 strains still form chains during broth culture growth, although the chains are not as long as those observed during growth on the agarose pads (**Figures 5 and S3**).

Since Clade 5 strains grow rapidly in rich media, we considered the possibility that the chaining phenotype might be mitigated by allowing more time for cell separation to occur after cell division. To test this possibility, we grew Clade 5 strains in CDDM minimal medium and analyzed their chaining properties [47]. While Clade 5 strains grew slower in CDDM medium relative to richer media (compare **Figure S4A** to **Figures 2 & S2**), the Clade 5 strains nevertheless formed chains in minimal medium (**Figure S4B**), with the exception of strain TAL29996 strain. Taken together, our results reveal that Clade 5 strains undergo cell separation less efficiently in a range of growth conditions relative to strains from other clades.

#### Cell length does not correlate with the propensity to sporulate.

We next wondered whether the propensity to form chains impacts the ability of Clade 5 strains to sporulate. Analyses in *Bacillus subtilis* suggest that smaller cells, such as those formed during stationary phase growth [48], are more likely to sporulate likely because they

concentrate proteins involved in the phosphorelay that induces sporulation [49, 50]. For example, a decrease in cell length in B. subtilis helps the kinase KinA reach the threshold concentration needed to trigger sporulation initiation. Although C. difficile lacks homologs of KinA and other components of the phosphorelay system [51], the longer cells generated by Clade 5 strains may be less likely to induce sporulation due to dilution of a currently unknown sporulation regulator. To test this hypothesis, we analyzed the propensity of Clade 5 strains to form spores when plated on 70:30 sporulation medium using phase-contrast microscopy and heat resistance assays. These analyses revealed that Clade 5 strains exhibit striking differences in sporulation frequency, with some strains exhibiting close to 100% sporulation levels, and others exhibiting levels closer to 20% (**Figures 6 & S5**). Interestingly, strain TAL29600 exhibited extremely low levels of sporulation (0.003%), and it continued to form chains during growth on 70:30 medium. In contrast, the other Clade 5 strains analyzed did not form long chains when grown on 70:30 sporulation medium, and the spores produced by these isolates exhibited similar lengths and proportions relative to the Clade 1 strain 630 (**Figure S6**). These data suggest that Clade 5 strains alter their cell length and propensity to form chains depending on the growth conditions encountered.

Consistent with this hypothesis, even though strain M120 forms long chains during growth in or on rich medium (**Figures 3 & S3**), it readily formed spores during growth on 70:30 medium ( $\sim$ 100% sporulation frequency, **Figure S5**). Notably, the average cell length for visibly sporulating Clade 5 cells was  $\sim$ 5-6  $\mu$ m (**Figure S8**) compared to the average  $\sim$ 11  $\mu$ m cell length measured for the Clade 5 strains in rich broth culture. This reduced cell length was observed even for Clade 5 strain TAL29600 (**Figure S8**), which sporulates poorly on 70:30 medium, indicating that there was little correlation between cell length and propensity to sporulate for the Clade 5 strains analyzed.

# Comparative genomics reveals that the chaining phenotype of Clade 5 strains is driven by *cmrRST* operon expression.

Given the phenotypic difference in chaining observed for the TAL29996 strain relative to the 8 other Clade 5 strains analyzed, we sought to gain insight into the mechanism driving this difference by comparing the genomes of five of the Clade 5 strains, including TAL29996. These

308

309

310

311

312

313

314

315

316

317

318

319

320

321

322

323

324

325

326

327

328

329

330

331

332

333

334

335

336

analyses revealed that the average nucleotide identity (ANI) for orthologous genes ranged between 99.83-99.99% (**Table S1**) and that the pan-genome between the five strains is 12%. Thus, all five strains are quite closely related. The pan-genome analysis revealed that, relative to the other four strains, TAL29996 is missing one duplication of blaR1, which encodes an integral membrane protein that senses beta-lactams, and a gene region predicted to be involved in nicotinate metabolism. To identify SNPs that might distinguish TAL29996 from the other strains, we used breseq [52]; the Clade 5 strain M120 genome sequence was used as the reference genome because it is the Clade 5 strain traditionally characterized [34, 53]. These analyses identified 10 SNPs that were unique to TAL29996, but none were obviously involved in regulating cell separation or peptidoglycan synthesis (Table S2). We next took a candidate approach to gain insight into why TAL29996 mediates cell separation more efficiently than the other Clade 5 strains by analyzing the orientation of the cmr switch, also known as the Cdi6 DNA invertible element [33, 54]. This phase-variable element affects the expression of the adjacent cmrRST operon, which encodes a non-canonical CmrRST signal transduction system that regulates cell chaining and colony morphology [33, 46, 54]. Cells from rough colonies form chains and are highly biased to the ON orientation of the cmr switch, whereas cells from smooth colonies do not form chains and are highly biased to the OFF orientation [33]. Although the sequence of the *cmr* switch is identical between the Clade 5 strains analyzed, including strain TAL29996, we found that the orientation of the cmr switch during growth in broth culture was markedly different for Clade 5 strain TAL29996. Specifically, qPCR analyses revealed that Clade 5 strains that form chains are biased towards the *cmr*-ON orientation (between 70-96% ON) (**Figure 7A**), whereas the *cmr*-ON orientation was markedly less frequent in the non-chaining strain TAL29996 (~20%, **Figure 7**). Since these analyses correlated the *cmr*-ON switch orientation to the chaining phenotype of Clade 5 strains, we tested whether knocking down the expression of the *cmrRST* operon using CRISPRi in strains that are biased towards the *cmr*-ON state would reduce their chaining properties. A plasmid targeting the cmrR gene using CRISPRi was introduced into the Clade 5 strains TAL28131, TAL30550, and TAL30574, which typically produce chains and are found predominantly in the *cmr*-ON state in rich broth culture (70-96%). Knocking down the expression of the cmrRST operon in all three strain backgrounds reduced their chaining

phenotypes under these conditions (**Figures 7B** & **S8**), indicating that the expression of the *cmrRST* operon in Clade 5 strains drives their propensity to form chains.

# Surface motility in Clade 5 strains relative to strains of other clades

Since the *cmr*-ON state has also been correlated with increased surface motility [33], we analyzed the surface motility of our Clade 5 strains. Consistent with prior reports [33], the primarily *cmr*-ON state strains exhibited greater and more uniform surface motility (**Figure 7C**), whereas the predominantly *cmr*-OFF state TAL29996 strain exhibited less and more asymmetric surface motility, with fractal-like extensions emerging from only a few sites. This asymmetric phenotype has previously been reported for the Clade 2 strain R20291, whose *cmr* switch is predominantly in the OFF position in liquid cultures but converts to the ON orientation during growth on plates [33]. These observations suggest that, even though TAL29996 is biased to the *cmr*-OFF orientation during broth culture growth, a subset of TAL29996 cells switch to the *cmr*-ON orientation during growth on BHIS agar, leading to the asymmetric spreading phenotype.

We next assessed whether additional Clade 1-4 strains exhibit surface motility. These analyses revealed that asymmetric motility was more frequently observed in Clade 2 strains, although Clade 2 strain Wup14 exhibited little surface motility (**Figure S9**). Clade 1 strains exhibited a range of surface motility, from high surface motility with strain 630 to lower surface motility with strain WU38 (**Figure S9**). While the data suggest that *cmr* switching in Clade 2 strains varies between strains during growth on agar medium, Clade 5 strains biased towards the *cmr*-ON state are more likely to exhibit surface motility. However, it is important to note that additional factors contribute to surface motility beyond expression of the *cmrRST* operon [33], since loss of pili can also decrease surface motility on plates [55]. Regardless, the data imply that the *cmr*-ON state promotes surface motility in Clade 5 strains.

#### Colonization and virulence properties of Clade 5 strains

Beyond the effects of the CmrRST system on cell chaining and surface motility, this system has also been shown to impact the virulence of the Clade 2 strain, R20291, in a hamster model of infection, with loss of *cmrR* reducing R20291's ability to cause disease and the *cmr*-

OFF orientation correlating with less severe disease in hamsters [33]. Since chaining in *Bacillus anthracis* strains promotes virulence [56], while chaining in *Enterococcus faecalis* promotes colonization [57], we compared the ability of Clade 5 strains to colonize mice and cause disease. Mice were infected with 10<sup>5</sup> spores of several Clade 5 strains and the Clade 1 strain 630 and the weight loss induced by these strains, their colonization levels, and orientation of the *cmr* switch over the course of the 14-day infection were assessed. For this latter analysis, we focused on strains TAL29600 and TAL29996 because they exhibited the highest and lowest *cmr*ON orientations, respectively, during growth in rich media (**Figure 7A**).

All Clade 5 strains tested colonized to relatively similar levels throughout the 14 days of the infection. Strain 630 also colonized mice to similar levels in the first two days of infection and then maintained colonization, albeit at 1-2 logs lower than the Clade 5 strains (**Figure 8A**). Interestingly, only the Clade 5 strain TAL29600 caused significant weight loss relative to the other strains on Days 2 through 4, although the Clade 1 strain 630 caused some weight loss on Day 3 (Figure 8B). This latter phenotype is consistent with prior reports of strain 630 causing only mild disease symptoms in the cefoperazone model of murine infection [58, 59]. Analyses of the cmr orientation revealed that the cmr-OFF orientation appeared to be selected for over the course of the infection. While the TAL29600 spore inoculum started off with ~30% cmr-ON frequency, the frequency of TAL29600 cells detected in the cmr-ON orientation decreased rapidly to < 5% cmr-ON by 24 hrs post-inoculation (**Figure 8C**). As the infection progressed, two of the 8 mice tested exhibited an increase in TAL29600 cells with the cmr-ON orientation (6-30% cmr-ON) (Figure S10). Conversely, the TAL29996 strain retained the ~1% cmr-ON frequency of the inoculum for the greater part of the 14-day infection (**Figure 8C**). Taken together, these analyses reveal that Clade 5 RT078 strains efficiently colonize mice but vary in their ability to cause disease. Furthermore, the ability of the Clade 5 strains to colonize or cause disease did not strongly correlate with their ability to form chains in broth culture.

#### **Discussion**

While Clade 5 strains are genetically distinct [10, 26] and more prevalent in animals than Clade 1-4 strains [12, 29, 30], the phenotypes that distinguish Clade 5 strains from Clade 1-4 strains are not well understood. By phenotypically characterizing *C. difficile* strains from

400

401

402

403

404

405

406

407

408

409

410

411

412

413

414

415

416

417

418

419

420

421

422

423

424

425

426

427

428

429

multiple clades using time-lapse microscopy, we discovered that Clade 5 strains have distinct growth properties from Clade 1-4 strains. Specifically, Clade 5 strains elongate more quickly (Figures 2, 4, S1) and form long chains more readily than strains from Clades 1-4, irrespective of media type or growth on a surface (Figures 2, 4, S2, and S4). In contrast, long chains were not observed in any of the Clade 1-4 strains, regardless of whether the cells were grown on agarose pads or in broth culture. Thus, Clade 5 strains undergo cell separation far less efficiently than strains from other clades during growth in rich media. While our analyses of Clade 5 strains were largely limited to the RT078 ribotype, we note that a prior report described an RT126 strain isolated from a patient experiencing multiple recurrences that also formed long chains [60]. Since the RT126 ribotype is closely related to the RT078 ribotype [12], it is likely that the chaining phenotype will be observed in other Clade 5 ribotypes. Our data indicate that the chaining phenotype of Clade 5 strains relates to their propensity to express the *cmrRST* operon [33, 46] because they favor the *cmr*-ON state (**Figure** 7). The non-chaining TAL29996 strain has a *cmr*-ON orientation frequency of 20%, whereas the 8 other Clade 5 strains have a strong bias for the *cmr*-ON orientation ( $\sim$ 70-96%, **Figure 7**). The chaining phenotype of Clade 5 strains prone to the *cmr*-ON state was enhanced during growth on a solid surface compared to broth culture (**Figures 4, 5**), consistent with prior analyses of the Clade 2 strain R20291, which exhibits greater cmrRST expression during growth on agar plates due to elevated c-di-GMP levels [46]. In addition, Clade 5 strains exhibit high levels of surface motility on agar plates, which is a *cmrRST*-induced phenotype in strain R20291 [33]. Finally, knocking-down the expression of the *cmrRST* operon in three Clade 5 strains biased to the *cmr*-ON state reduced their propensity to form chains (**Figures 7 & S8**). These findings lead to the question of what benefit *cmrRST* expression might confer to Clade 5 strains. In the Clade 2 R20291 strain, cmrRST expression is negatively correlated with flagellar motility, and growth conditions that favor flagellar motility select against the cmr-ON state [33]. Since Clade 5 strains lack flagellar motility [12], it is tempting to hypothesize that they are "primed" to form chains as a method to promote motility. Analyzing the regulation of c-di-GMP in different growth conditions in Clade 5 strains, particularly for TAL29996 relative to the other strains, will likely provide insight into the mechanisms that drive cmrRST expression, chaining, and surface motility in Clade 5 strains and the importance of these properties to these strains.

431

432

433

434

435

436

437

438

439

440

441

442

443

444

445

446

447

448

449

450

451

452

453

454

455

456

457

458

459

strains to be detected.

While the propensity of Clade 5 strains to form chains in a *cmrRST*-dependent manner might be expected to promote colonization or disease in mice based on studies of other Grampositive pathogens [56, 57], we found that the frequency of cmr-ON cells decreases during the first 4 days of infection for strain TAL29600 (Figure 8). This suggests that there may be a selection against cmr-ON cells during the initial stages of murine colonization. Consistent with this hypothesis, a decrease in cmr-ON orientation was observed for Clade 2 strain R20291 during infection of hamsters [33]. However, since the frequency of *cmr*-ON TAL29600 cells increased in some mice at later stages of colonization (Figure 8), our data imply that the invertibility of the cmrRST switch region may promote C. difficile's ability to adapt to different growth conditions. While it is possible that high levels of c-di-GMP during infection induce the expression of the *cmrRST* operon expression during murine infection [46], assessing whether Clade 5 strains form long chains during murine infection, for example, using fluorescence in situ hybridization [61, 62] or using transcriptional reporters to visualize the expression of the cmrRST operon at the single-cell level during infection would provide insight into these questions. Indeed, the avirulence of most Clade 5 strains analyzed during murine infection (**Figure** 8) was somewhat surprising given that all of these strains were isolated from human patients experiencing CDI-related disease symptoms (**Table 1**). To our knowledge, very few Clade 5 strains have been analyzed during murine infection, with one study observing minor disease symptoms in mice for two Clade 5 strains three days post-infection, despite one of the strains causing severe disease in humans [20]. Interestingly, RT078 Clade 5 strains frequently cause asymptomatic infections in agricultural animals [32, 63] and mice may be important vectors of transmission in these settings [64, 65]. Thus, it is possible that Clade 5 strains are adapted for colonization rather than virulence in non-human systems. Consistent with this hypothesis, we found that the Clade 5 strains persist at high levels in the murine gut over time compared to the Clade 1 strain 630 (**Figure 8**, p < 0.005). Identifying factors that allow Clade 5 strains to grow more quickly would provide insight into whether their faster growth rate promotes their persistence in mice. It is also possible that increasing the inoculum could have allowed for a greater degree of disease severity to be observed and differences in virulence between the

461

462

463

464

465

466

467

468

469

470

471

472

473

474

475

476

477

478

479

480

481

482

483

484

485

486

487

488

489

490

Interestingly, the chain length of Clade 5 strains did not correlate with their propensity to sporulate (**Figure 6**). The Clade 5 strains tested varied markedly in their sporulation frequencies, with most strains forming spores at frequencies >30% unlike strain TAL29600, which sporulates ~5,000-fold less efficiently than the other Clade 5 strains (**Figure 6**). While little is known about the mechanisms regulating sporulation initiation outside of strains 630 and R20291, analyses of strain TAL29600, which sporulates poorly under laboratory conditions (**Figure 6**), could provide insight into the molecular determinants of sporulation initiation in Clade 5 strains. For example, differences in gene presence or polymorphisms in several c-di-GMP-related genes were observed in TAL29600 relative to the other Clade 5 strains (**Table S2**), and c-di-GMP has been implicated in regulating sporulation initiation events through unknown mechanisms [66, 67]. Our time-lapse microscopy analyses further revealed that a notable delay between cell division and cell separation is common to C. difficile strains, irrespective of their propensity to form long chains, because chains of two cells were frequently observed for Clades 1-4 and Clade 5 strain TAL29996 (Figures S3 & 4). Notably, these two-cell chains were typically segmented by DeLTA as a single cell because cell separation had not initiated, i.e. no invagination was detected (Figure 4, red dot). The loose coordination between cell division and cell separation in C. difficile relative to other bacteria likely relates to the absence of FtsEX homologs in C. difficile. In diverse bacteria, the FtsEX complex couples septal PG synthesis with PG hydrolases that mediate cell separation to result in a fast splitting of recently divided cells [68-71]. While it remains unclear whether coordination between cell division and cell separation exists in C. difficile, recent work has identified novel factors that control chaining in C. difficile. The CwlA peptidoglycan hydrolase mediates cell separation in C. difficile [72], and its export and thus activity is controlled by the Ser/Thr kinase PrkC [72]. The septum-localizing MldA or MldB proteins also promote chaining in C. difficile through unknown mechanisms [73], so future work could address whether the inefficient cell separation phenotype of Clade 5 strains is due to decreased CwlA export or MldA/MldB levels. Importantly, these insights into the basic physiology of C. difficile were enabled by our development of a facile method for conducting time-lapse microscopy under anaerobic conditions. Since the growth chamber set-up involves commercially available GeneFrames and open-source software for conducting automated image analyses of time-lapse microscopy data

 [43, 44], the methods described in this manuscript can be applied to many anaerobic systems for studying the growth properties of diverse organisms and the impact of different growth conditions and mutant backgrounds on these properties. Our anaerobic set-up could be further coupled with recently developed, fluorogen-activated anaerobic imaging tags [74] to facilitate single-cell analyses of gene-specific transcription during anaerobic growth and dynamic protein localization studies [75]. Thus, there are many potential applications for the simple methods described here for studying the growth of anaerobes over time at the single-cell level.

#### **Materials and Methods**

Bacterial strains and growth conditions

All *C. difficile* strains were grown on brain heart infusion (BHIS) medium supplemented with 0.5% w/v yeast extract and 0.1% w/v L-cysteine with taurocholate (TCA; 0.1% w/v; 1.9 mM). Strains were sub-cultured into tryptone yeast extract (TY) broth supplemented with 0.1% w/v L-cysteine (TYC medium) prior to inoculation onto the time-lapse microscopy agarose pads. All strains were grown at 37°C under anaerobic conditions using a gas mixture of 85% hydrogen, 5% CO2, and 10% H2. For time-lapse experiments, 1.5% agarose pads supplemented with TYC medium were used as described above. Sporulation analyses were carried out on 70:30 medium (70% BHIS and 30% SMC) for 24h as described previously [76].

# Anaerobic time-lapse imaging of C. difficile growth

All imaging was carried out on a Leica DMi8 inverted microscope with a HC plan apochromat 63x 1.4 NA oil immersion phase contrast objective. Fluorescent membrane staining experiments were done with a Lumencor Spectra X light source, coupled with an XLED-QP quadruple-band dichroic beam-splitter (Leica) (transmission: 415, 470, 570, and 660 □ nm) along with an external emission filter wheel (Leica). FM4-64 was excited using a 470nm LED through a 470/20nm excitation filter and emitted light was filtered through a 590/50nm emission filter and captured with a Leica DFC9000GTC sCMOS camera. All experiments were carried out at 37°C using a microscope incubation system (Pecon), Leica Adaptive Focus Control hardware autofocus, and a high precision stage (Pecon) were used for all imaging experiments.

For time-lapse imaging of C. difficile growth, all bacterial strains were grown in 2 mL liquid TY medium to a turbid OD600 > 2-3; after 2 hours of growth, bacteria were diluted 1:100 for Clade 5 strains and all other strains were diluted 1:50 in fresh media and grown to mid-log phase (OD600 0.4-0.7).

An imaging chamber with a gas-tight seal was constructed using a 125  $\mu$ L Gene Frame (Thermo Fisher) adhered to a glass slide generating a well for growth medium. The slide was then transferred to the anaerobic chamber. In the anaerobic chamber, the gene frame was filled with 500 $\mu$ l 1.5% Top vision low melting point agarose and tryptone yeast extract media containing 0.1% w/v L-cysteine to scavenge oxygen and maintain anaerobic conditions. While the agarose was molten, a second clean slide was placed over the top and the agar pad was placed on a frozen small freezer block (for holding PCR strip tubes) for 10-30 minutes until the agarose-media mixture was solid. For experiments using FM4-64, agarose pads were made the same way, with the addition of FM4-64 to a final concentration of 1  $\mu$ g/mL directly to the agarose/media solution prior to making the agar pad.

The agar pad was dried for 5-10 minutes until visible liquid on the surface of the pad was evaporated. 1  $\mu$ L of mid-log cells were spotted on the pad, dried, and a #1.5 coverslip (VWR) was adhered to the Gene Frame. The cells were imaged at 37°C until they reached confluency in the field of view. This was anywhere from 2.5 hours for Clade 5 strains to 6 hours for Clades 1-4 for all experiments with images taken at 5-minute intervals.

Image analysis, computing hardware, and statistical analysis.

All movie frames were trimmed to the point when cells were not overlapping and out of focus regions were cropped. The resulting images were analyzed using the Python library

- DeLTA 2.0 [43, 44]. All image and data analyses were done on a PC running Windows 10
- equipped with an AMD Ryzen 5900HX 8-core CPU, 32GB DDR4 RAM, 2 1TB NVME SSDs,
- and an NVIDIA RTX3080 GPU with 16GB VRAM. Analysis of the output data and data
- visualizations were done in Python using Matplotlib/Seaborn, Pandas, Numpy, Scipy, and the
- 551 Statannotations library.

567568

581 582

- 553 Septum detection during live-cell microscopy
- The image processing starts with the masks generated using DeLTA. First, we performed erosion
- on the mask with a disk of radius of 1 pixel to avoid effects of membrane fluorescence. The
- 556 photo was cropped following the eroded mask contour. Hence, only the interior of the contour
- was considered. Pixel values were rescaled such that the minimum pixel value of inner pixels
- was mapped to 0 and the maximum was mapped to 255. We set a threshold intensity as the pixel
- value of the 95% quantile of pixel intensities. The image was slightly blurred by convolution
- with a Gaussian filter with standard deviation of 2 pixels. The septum corresponds to the
- contours found after performing an adaptive thresholding based on thresholds defined using a
- Gaussian-weighted method. This thresholding was performed using the open cv2 library in
- Python. The resultant contours were manually verified from videos generated using the tracking
- from the outputs from DeLTA. The manual validation mainly involved filling in the time points
- where the algorithm missed a ring that was visible in the video. We did not assume the existence
- of a ring if the algorithm did not detect it in a previous frame.
  - Cell length estimation
- We measured the cell projected area from the DeLTA contours of the images as the pixel amount
- of the contours. However, estimating cell length was challenging because some cells were very
- long and bent. To overcome this problem, we selected 30 images of three different cells (from
- strains 630, TAL3050 and TAL28131) that were straight and had different lengths. For these
- 573 cells, we calculated the cell length as the longest side of the minimum bounding rectangle of the
- 574 contour. From these lengths of straight cells, we also estimated the best cell width as the average
- of the projected area divided by the length. Considering the extreme cell length, the effects of the
- 576 rounded tips were negligible and the rectangle shape adequately approximated length. We
- verified that this mean value showed low variability for the three strains. Then, we used this
- width value to estimate the length of all the cells, including the bent ones, by dividing their
- projected area by the width. This way, we obtained a consistent measure of cell length that was
- independent of bending.
  - Elongation rate estimation
- We tracked cell size over time and identified the division points as the ones where the cell size
- 584 (projected area) dropped by more than 30% compared to the current cell size value. We fitted an
- exponential function (with base e) of time to the data points between two divisions and estimated
- the elongation rate from the exponent of the best fit. We expressed the elongation rate in
- doublings/hr, which means how many times the cell size doubles in one hour. For example, an
- elongation rate of 2 doubling/hr means that the cell size doubles two times in 1 hr, which
- corresponds to an exponent of 2ln(2) 1/hr. For the statistics, we only included the elongation
- rates that had a high quality of fit, with an R2 coefficient greater than 0.9.
  - Bulk growth measurements

- 593 Starter cultures were grown until early stationary phase in BHIS (or TYC medium as indicated)
- then diluted 1:50 into BHIS (or TYC medium). For the CDDM growth analyses, starter cultures
- were prepared in CDDM medium at a relatively high density and then back-diluted 1:25 into
- 596 CDDM. When the cultures (for all three media conditions) reached an  $OD_{600}$  of 0.5, they were
- diluted 1:50 into 200 µL of either BHIS, TYC, or CDDM in a flat 96 well polystyrene plate
- (CellTreat). The OD<sub>600</sub> was analyzed every 15 min for 24 hrs in a BioTek Epoch plate reader
- with shaking. Bulk growth measurements are based on a minimum of three independent
- 600 replicates across a minimum of 2 experiments. The growth rate was calculated from the linear
- range of the growth curves, between 105 min to 180 min of growth.
  - Cell wall labeling

611

619

625

- HADA (Tocris Bioscience) was added to exponentially growing cell culture to a final
- concentration of 50-100 µM and incubated for ~2 mins before cell fixation. Cells were fixed as
- previously described [77]. Briefly, 500 μL of cell suspension was added to 120 μL of a 5X
- 607 fixation solution containing paraformaldehyde and NaPO<sub>4</sub> buffer. Samples were mixed and
- incubated in the dark for 30 min at room temperature, followed by 30 min on ice. Fixed cells
- were washed three times in phosphate-buffered saline (PBS) and resuspended in ~50 µL of PBS.
- 610 Cells were imaged within 72 hours after fixation.
- 612 Sporulation assays.
- Starter cultures were grown until early stationary phase in BHIS then diluted 1:50 into BHIS.
- When the cultures reached an  $OD_{600}$  between 0.35 and 0.75,  $120 \square \mu L$  of the culture was spread
- onto 70:30 (70% SMC media and 30% BHIS media) agar plates (40 ml media per plate) and
- then incubated for 20-24 hrs before the sporulating cells were scraped from the plate into
- phosphate-buffered saline (PBS). Sporulation levels were visualized by phase-contrast
- microscopy as previously described [78].
- 620 Heat resistance assay.
- Heat-resistant spore formation was measured 20-24 hrs after sporulation was induced on 70:30
- agar plates as previously described [76]. The percent sporulation of given culture represents the
- ratio of heat-resistant colony-forming units (CFUs) to total CFUs. Percent sporulation was
- determined from a minimum of 3 biological replicates.
- 626 Spore purification.
- Spores were purified as previously described [79] by scraping up sporulating cells incubated on
- 628 70:30 medium for 3 days into ice-cold H<sub>2</sub>O. The cells were washed several times in ice-water
- over the course of a day and incubated on ice overnight. The following morning, the sample was
- pelleted, and cells were suspended in 1 X DNAse buffer (New England Biolabs) and then treated
- with DNAse (New England Biolabs) for 30 min at 37°C. The samples were washed one more
- time before being resuspended in 20% Histodenz and then layered onto a 50% Histodenz layer.
- The resulting mixture was pelleted, and the supernatant was aspirated off using a vacuum
- aspirator. The pelleted spores were washed in ice-cold water 2-3 times and the optical density of
- the purified spores was measured.
- 637 Genomic DNA preparation.
- 638 Starter cultures were grown until early stationary phase in BHIS then back-diluted 1:50 into
- BHIS and grown until an  $OD_{600}$  of around 0.7-0.8 was reached. 10 mL of the culture was

- 640 pelleted and then frozen at -80°C. After thawing the sample, it was resuspended in a 25% 641 sucrose TE buffer (10 mM Tris, 1mM EDTA), incubated with 100 mg/mL lysozyme for 37°C 642 for 1 hr. After the cultures tarted to lyse, proteinase K, RNAse A, EDTA, Sarkosyl, and NaCl 643 was added. Phenol:Chloroform:IAA (25:24:1) was added to extract proteins, gently mixed, and 644 then the sample was pelleted to separate the phenol and aqueous layer. The aqueous layer was 645 then added to Chloroform:IAA (24:1), mixed gently, then centrifuged. The aqueous layer was 646 then precipitated using isopropanol and incubated at -20°C for a minimum of 15 min. The 647 precipitated DNA was pelleted and then washed with 70% ethanol. The pellet was air dried and 648 then gently resuspended in 10 mM Tris pH 8.0 elution buffer.
  - Genomic analyses.

661 662

663

664

665

666

667

668 669

670

671

672

673

- 651 Genomic DNA was sequenced by MiGS at the University of Pittsburgh (now SeqCenter) 652 according to their standard protocol. Libraries were sequenced on an Illumina NextSeq 500 653 platform to generate paired-end 150 bp reads. Illumina reads of RT078 genomes were assembled 654 into contigs using SPAdes (v3.13.0),[80] and genes were called and annotated using Prokka 655 (v1.11) [81]. Assembled and annotated contigs of five RT078 strains (TAL28131, TAL29600, 656 TAL29996, TAL30550, TAL30574) were applied for pangenomic analysis. Default settings 657 were used based on the Anvi'o workflow for microbial pangenomcis with adjustments for minbit 658 as 0.5 and mcl-inflation as 10[82-84]. For SNPs analyses, reads of five RT078 genomes were 659 aligned to the reference M120 and variants were called by breseq (v. 0.38.1) by default 660 settings.[85]
  - *qPCR* analyses.
  - Each genomic DNA sample was analyzed by qPCR with primers that amplify the cmr-ON sequence orientation, the cmr-OFF orientation, or the reference gene rpoA [33]. Each 20-µL qPCR reaction consisted of 100 ng genomic DNA, 100 nM primers, and SensiMix™ SYBR reagents (Bioline). The reactions were run on a LightCycler® 96 (Roche Diagnostics), and cmr switch orientation frequencies were calculated as described previously [46].
  - Surface motility assays
  - Starter cultures were grown until early stationary phase in BHIS then back-diluted 1:50 into BHIS and grown until an  $OD_{600}$  of 0.5 was reached. 10 µL of the exponential-phase cultures were then spotted onto BHIS plates and incubated at 37°C for 5 days after which the plates were scanned using a flatbed scanner.
  - *Mouse infection experiments*
- 676 Mouse experiments were performed under the guidance of veterinary staff within the Tufts 677 Comparative Medicine Services (TCMS) core. All animal studies were done with prior approval from the Tufts Institutional Animal Care and Use Committee (IACUC protocol #B2024-30). 678 679 Conventional 7-week-old C57BL/6 female mice from Jackson Laboratories were housed in a 680 sterile (autoclaved cage and bedding) large cage (24"x17") with autoclaved water and irradiated 681 food (Teklad 2918) for 10 days to allow for normalization of microbiota across mice through 682 coprophagy. After the 10-day normalization period, mice were started on cefoperazone, which 683 was added to their water at a concentration of 0.5 mg/ml. Mice were allowed to drink the 684 cefoperazone water ad libitum for 10 days, after which they were placed back on sterile water 685
  - without antibiotic. After a 2-day period of being on normal sterile water, mice were weighed and

686 given a single dose of clindamycin (10mg/kg) via intraperitoneal injection. Immediately after IP 687 injection, mice were moved to standard-size autoclaved mouse cages (4 mice per cage) with 688 sterile food and water. 24 hours following the clindamycin injection, mice were inoculated with 689 1 x 10<sup>5</sup> spores of C. difficile (in 1xPBS) via oral gavage using a metal, reusable needle. Mice 690 were weighed by being placed in a plastic Nalgene cup on top of a scale. Fecal pellets were collected just prior to oral gavage to ensure no prior C. difficile colonization and to note a 691 692 baseline weight. Following inoculation, mice were weighed to monitor % weight change over 693 time on days 1-4, 7, and 14. Fecal pellets were collected in duplicate on the same days for C. 694 difficile CFU enumeration and qPCR for detection of cmr switch orientation. On day 14, a 695 terminal weight was taken, and a fecal pellet was collected, followed by sacrifice via CO<sub>2</sub> 696 inhalation with cervical dislocation as secondary method of euthanasia. Two experimental 697 replicates were completed using 4 mice per group, resulting in a total of 8 mice per condition. 698

# C. difficile CFU enumeration from mouse fecal pellets

C. difficile engraftment in mice was monitored over a 14-day period. Fecal pellets were collected from mice on days 0-4, 7, and 14. Each pellet was weighed and then suspended in 1x PBS. 10  $\mu$ L of the suspension was then serially diluted 1:10 in 1x PBS in a 96 well plate, and 5  $\mu$ L was spotted onto TCCFA agar to select for C. difficile, such that the dilutions plated were 2 x 10<sup>3</sup> – 2 x 10<sup>7</sup>. C. difficile colonies were counted 24 hours after plating to allow for sufficient growth. C. difficile CFUs were normalized by gram of fecal material.

# Data accessibility statement

The data set and data processing scripts are publicly available at <a href="https://doi.org/10.5281/zenodo.13352469">https://doi.org/10.5281/zenodo.13352469</a> [86]. Genomes are available from NCBI under the BioProject ID PRJNA1238863.

# Acknowledgements

- We are grateful to Dr. Cheleste Thorpe, Dr. Eric Pamer, Dr. Bruno Dupuy, Dr. Lynn Bry, and Dr.
- 715 Trevor Lawley for providing the strains used in this study.
- 717 Funding

699

700

701

702

703

704

705

706 707

708

709

710

711 712 713

716

- 718 This work was supported by NIAID grants R21 AI153853 (A Shen, BBA, and MJD), R01
- 719 AI122232 (A Shen), R01 AI143638 (RT), and T32 AI007422 (NVD) and NIGMS grants R35
- GM148351 (A Singh), and T32 GM007310 (JWR). The funders had no role in study design, data
- 721 collection and analysis, decision to publish, or preparation of the manuscript.

# Table 1. Clostridioides difficile clinical isolates used in this study

Strain Name	Clade	Ribotype	ST group	Source	Reference
630	1	012	2	Zurich, 1982 (Sanger Institute)	[87]
BBL2	1	012	2	Memorial Sloan Kettering	[20]
WU38	1	012	2	Barnes-Jewish Hospital	[20]
190B	1	087	46	Memorial Sloan Kettering	[20]
R20291	2	027	1	London, 2006 (Sanger Institute)	[88]
Wup14	2	027	1	Barnes-Jewish Hospital	[20]
BBL4	2	027	1	Memorial Sloan Kettering	[20]
186A	2	027	1	Memorial Sloan Kettering	[20]
E15	3	075	unknown	France (Bruno Dupuy/ Lynn	[89, 90]
				Bry)	
BI1	3	unknown	unknown	Bruno Dupuy/ Lynn Bry	This study
95-978	3	unknown	unknown	Bruno Dupuy/ Lynn Bry	This study
M68	4	017	81	Dublin, 2006 (Sanger Institute)	[53]
1002	4	unknown	39	Memorial Sloan Kettering [20	
M120	5	078	11	UK, 2007 (Sanger Institute) [53	
TAL28131	5	078	11	NY Presbyterian/Weill Cornell [91]	
				Medical Center	
TAL29600	5	078	11	RM Alden Research Lab	[91]
TAL29996	5	078	11	Vines VA Hospital [91]	
TAL30550	5	078	11	Mayo Clinic [91]	
TAL30574	5	078	11	Tufts Medical Center	[91]
V48	5	078	11	Brigham & Women's Hospital	This study
139b	5	078	11	Memorial Sloan Kettering	[20]
WU66	5	078	11	Barnes-Jewish Hospital	[20]

Memorial Sloan Kettering Cancer Center (MSK), Barnes-Jewish Hospital (BJH)

Table 2: Cell size and growth rate statistics for the studied strains.

Strain Name	Clade	Mean Growth rate	Mean Cell Length (um)	Mean Chain Length (um)
630	1	$1.63 \pm 0.02$	$8.5 \pm 2.2$	$12.5 \pm 3.5$
R20291	2	$1.88 \pm 0.01$	not measured	$11.7 \pm 3.2$
E15	3	$1.92 \pm 0.01$	not measured	$13.6 \pm 4.2$
M68	4	$1.64 \pm 0.01$	not measured	$13.7 \pm 4.3$
M120	5	$2.15 \pm 0.01$	not measured	$21.8 \pm 10.2$
TAL29996	5	$2.15 \pm 0.02$	$9.4 \pm 2.7$	$13.7 \pm 3.9$
TAL28131	5	$2.17 \pm 0.02$	$11.2 \pm 3.3$	$19.7 \pm 6.9$
V48	5	2.10 ±0.02	$10.8 \pm 3.7$	$19.4 \pm 8.5$
TAL30550	5	$2.05 \pm 0.04$	11.8 ±.3.3	$27.3 \pm 9.8$

TAL29600 5 $2.11 \pm 0.02$ $14.0 \pm 4.4$ $29.1 \pm 13.1$		5	$2.11 \pm 0.02$		29.1± 13.1
---	--	---	-----------------	--	------------

The  $\pm$  interval represents the 95% confidence interval of the mean growth rate. The standard deviation (S.D) is provided.

#### References

737

- 739 1. Desai K, Gupta SB, Dubberke ER, Prabhu VS, Browne C, Mast TC. Epidemiological and
- 740 economic burden of *Clostridium difficile* in the United States: estimates from a modeling
- 741 approach. BMC Infect Dis. 2016;16:303. Epub 20160618. doi: 10.1186/s12879-016-1610-3.
- PubMed PMID: 27316794; PubMed Central PMCID: PMCPMC4912810.
- 743 2. Guh AY, Mu Y, Winston LG, Johnston H, Olson D, Farley MM, et al. Trends in U.S.
- Burden of *Clostridioides difficile* Infection and Outcomes. N Engl J Med. 2020;382(14):1320-30.
- 745 doi: 10.1056/NEJMoa1910215. PubMed PMID: 32242357; PubMed Central PMCID:
- 746 PMCPMC7861882.
- 3. Shen A. *Clostridioides difficile* Spore Formation and Germination: New Insights and
- Opportunities for Intervention. Annu Rev Microbiol. 2020;74:545-66. doi: 10.1146/annurev-
- 749 micro-011320-011321. PubMed PMID: 32905755.
- Abt MC, McKenney PT, Pamer EG. Clostridium difficile colitis: pathogenesis and host
- defence. Nat Rev Microbiol. 2016. doi: 10.1038/nrmicro.2016.108. PubMed PMID: 27573580.
- 752 5. Theriot CM, Young VB. Interactions Between the Gastrointestinal Microbiome and
- 753 Clostridium difficile. Annu Rev Microbiol. 2015;69:445-61. doi: 10.1146/annurev-micro-
- 754 091014-104115. PubMed PMID: 26488281.
- 755 6. Kordus SL, Thomas AK, Lacy DB. *Clostridioides difficile* toxins: mechanisms of action
- and antitoxin therapeutics. Nat Rev Microbiol. 2022;20(5):285-98. Epub 20211126. doi:
- 757 10.1038/s41579-021-00660-2. PubMed PMID: 34837014; PubMed Central PMCID:
- 758 PMCPMC9018519.
- 759 7. Maroo S, Lamont J. Recurrent *Clostridium difficile*. Gastroenterology. 2006;130(4):1311-
- 760 6. doi: 10.1053/j.gastro.2006.02.044.
- 761 8. Zanella Terrier MC, Simonet ML, Bichard P, Frossard JL. Recurrent Clostridium difficile
- infections: the importance of the intestinal microbiota. World journal of gastroenterology: WJG.
- 763 2014;20(23):7416-23. doi: 10.3748/wjg.v20.i23.7416. PubMed PMID: 24966611; PubMed
- 764 Central PMCID: PMC4064086.
- 765 9. Knight DR, Elliott B, Chang BJ, Perkins TT, Riley TV. Diversity and Evolution in the
- Genome of *Clostridium difficile*. Clin Microbiol Rev. 2015;28(3):721-41. doi:
- 767 10.1128/CMR.00127-14. PubMed PMID: 26085550; PubMed Central PMCID:
- 768 PMCPMC4475645.
- 769 10. Knight DR, Imwattana K, Kullin B, Guerrero-Araya E, Paredes-Sabja D, Didelot X, et al.
- Major genetic discontinuity and novel toxigenic species in *Clostridioides difficile* taxonomy.
- 771 Elife. 2021;10. Epub 20210611. doi: 10.7554/eLife.64325. PubMed PMID: 34114561; PubMed
- 772 Central PMCID: PMCPMC8241443.
- 773 11. Norsigian CJ, Danhof HA, Brand CK, Midani FS, Broddrick JT, Savidge TC, et al.
- 774 Systems biology approach to functionally assess the *Clostridioides difficile* pangenome reveals
- genetic diversity with discriminatory power. Proc Natl Acad Sci U S A.
- 776 2022;119(18):e2119396119. Epub 20220427. doi: 10.1073/pnas.2119396119. PubMed PMID:
- 777 35476524; PubMed Central PMCID: PMCPMC9170149.
- 778 12. Knight DR, Kullin B, Androga GO, Barbut F, Eckert C, Johnson S, et al. Evolutionary
- and Genomic Insights into *Clostridioides difficile* Sequence Type 11: a Diverse Zoonotic and
- Antimicrobial-Resistant Lineage of Global One Health Importance. mBio. 2019;10(2). Epub
- 781 20190416. doi: 10.1128/mBio.00446-19. PubMed PMID: 30992351; PubMed Central PMCID:
- 782 PMCPMC6469969.

- 783 13. Seth-Smith HMB, Biggel M, Roloff T, Hinic V, Bodmer T, Risch M, et al. Transition
- From PCR-Ribotyping to Whole Genome Sequencing Based Typing of *Clostridioides difficile*.
- 785 Front Cell Infect Microbiol. 2021;11:681518. Epub 20210601. doi: 10.3389/fcimb.2021.681518.
- 786 PubMed PMID: 34141631; PubMed Central PMCID: PMCPMC8204696.
- 787 14. Dingle KE, Elliott B, Robinson E, Griffiths D, Eyre DW, Stoesser N, et al. Evolutionary
- history of the *Clostridium difficile* pathogenicity locus. Genome Biol Evol. 2014;6(1):36-52. doi:
- 789 10.1093/gbe/evt204. PubMed PMID: 24336451; PubMed Central PMCID: PMCPMC3914685.
- 790 15. Mengoli M, Barone M, Fabbrini M, D'Amico F, Brigidi P, Turroni S. Make It Less
- 791 difficile: Understanding Genetic Evolution and Global Spread of *Clostridioides difficile*. Genes
- 792 (Basel). 2022;13(12). Epub 20221124. doi: 10.3390/genes13122200. PubMed PMID: 36553467;
- 793 PubMed Central PMCID: PMCPMC9778335.
- 794 16. Clements AC, Magalhaes RJ, Tatem AJ, Paterson DL, Riley TV. Clostridium difficile
- 795 PCR ribotype 027: assessing the risks of further worldwide spread. Lancet Infect Dis.
- 796 2010;10(6):395-404. doi: 10.1016/S1473-3099(10)70080-3. PubMed PMID: 20510280; PubMed
- 797 Central PMCID: PMCPMC7185771.
- 798 17. Endres BT, Begum K, Sun H, Walk ST, Memariani A, Lancaster C, et al. Epidemic
- 799 Clostridioides difficile Ribotype 027 Lineages: Comparisons of Texas Versus Worldwide Strains.
- 800 Open Forum Infect Dis. 2019;6(2):ofz013. Epub 20190209. doi: 10.1093/ofid/ofz013. PubMed
- 801 PMID: 30793006; PubMed Central PMCID: PMCPMC6368847.
- 802 18. McDonald LC, Killgore GE, Thompson A, Owens RC, Jr., Kazakova SV, Sambol SP, et
- al. An epidemic, toxin gene-variant strain of *Clostridium difficile*. N Engl J Med.
- 804 2005;353(23):2433-41. Epub 20051201. doi: 10.1056/NEJMoa051590. PubMed PMID:
- 805 16322603.
- 806 19. Dong Q, Lin H, Allen MM, Garneau JR, Sia JK, Smith RC, et al. Virulence and genomic
- diversity among clinical isolates of ST1 (BI/NAP1/027) Clostridioides difficile. Cell Rep.
- 808 2023;42(8):112861. Epub 20230730. doi: 10.1016/j.celrep.2023.112861. PubMed PMID:
- 809 37523264; PubMed Central PMCID: PMCPMC10627504.
- 810 20. Lewis BB, Carter RA, Ling L, Leiner I, Taur Y, Kamboj M, et al. Pathogenicity Locus,
- 811 Core Genome, and Accessory Gene Contributions to *Clostridium difficile* Virulence. mBio.
- 812 2017;8(4). Epub 20170808. doi: 10.1128/mBio.00885-17. PubMed PMID: 28790208; PubMed
- 813 Central PMCID: PMCPMC5550754.
- 814 21. Merrigan M, Venugopal A, Mallozzi M, Roxas B, Viswanathan VK, Johnson S, et al.
- Human hypervirulent *Clostridium difficile* strains exhibit increased sporulation as well as robust
- 816 toxin production. J Bacteriol. 2010;192(19):4904-11. Epub 20100730. doi: 10.1128/JB.00445-10.
- 817 PubMed PMID: 20675495; PubMed Central PMCID: PMCPMC2944552.
- Nhu NTQ, Lin H, Pigli Y, Sia JK, Kuhn P, Snitkin ES, et al. Flagellar switch inverted
- 819 repeat impacts flagellar invertibility and varies *Clostridioides difficile* RT027/MLST1 virulence.
- bioRxiv. 2024. Epub 20240924. doi: 10.1101/2023.06.22.546185. PubMed PMID: 39386689;
- PubMed Central PMCID: PMCPMC11463649.
- 822 23. Shaw HA, Preston MD, Vendrik KEW, Cairns MD, Browne HP, Stabler RA, et al. The
- recent emergence of a highly related virulent *Clostridium difficile* clade with unique
- characteristics. Clin Microbiol Infect. 2020;26(4):492-8. Epub 20190913. doi:
- 825 10.1016/j.cmi.2019.09.004. PubMed PMID: 31525517; PubMed Central PMCID:
- 826 PMCPMC7167513.
- 24. Li C, Harmanus C, Zhu D, Meng X, Wang S, Duan J, et al. Characterization of the
- virulence of a non-RT027, non-RT078 and binary toxin-positive *Clostridium difficile* strain

- associated with severe diarrhea. Emerg Microbes Infect. 2018;7(1):211. Epub 20181212. doi:
- 830 10.1038/s41426-018-0211-1. PubMed PMID: 30542069; PubMed Central PMCID:
- 831 PMCPMC6291415.
- 832 25. Imwattana K, Rodriguez C, Riley TV, Knight DR. A species-wide genetic atlas of
- antimicrobial resistance in *Clostridioides difficile*. Microb Genom. 2021;7(11). doi:
- 834 10.1099/mgen.0.000696. PubMed PMID: 34793295; PubMed Central PMCID:
- 835 PMCPMC8743556.
- 836 26. Kumar N, Browne HP, Viciani E, Forster SC, Clare S, Harcourt K, et al. Adaptation of
- host transmission cycle during *Clostridium difficile* speciation. Nat Genet. 2019;51(9):1315-20.
- 838 Epub 20190812. doi: 10.1038/s41588-019-0478-8. PubMed PMID: 31406348.
- 839 27. Jain C, Rodriguez RL, Phillippy AM, Konstantinidis KT, Aluru S. High throughput ANI
- analysis of 90K prokaryotic genomes reveals clear species boundaries. Nature Comm.
- 841 2018;9(1):5114. Epub 20181130. doi: 10.1038/s41467-018-07641-9. PubMed PMID: 30504855;
- PubMed Central PMCID: PMCPMC6269478.
- 843 28. Knetsch CW, Kumar N, Forster SC, Connor TR, Browne HP, Harmanus C, et al.
- 844 Zoonotic Transfer of *Clostridium difficile* Harboring Antimicrobial Resistance between Farm
- 845 Animals and Humans. J Clin Microbiol. 2018;56(3). Epub 20180222. doi: 10.1128/JCM.01384-
- 17. PubMed PMID: 29237792; PubMed Central PMCID: PMCPMC5824051.
- Hensgens MP, Keessen EC, Squire MM, Riley TV, Koene MG, de Boer E, et al.
- 848 Clostridium difficile infection in the community: a zoonotic disease? Clin Microbiol Infect.
- 849 2012;18(7):635-45. Epub 20120427. doi: 10.1111/j.1469-0691.2012.03853.x. PubMed PMID:
- 850 22536816.
- 30. Goorhuis A, Bakker D, Corver J, Debast SB, Harmanus C, Notermans DW, et al.
- 852 Emergence of *Clostridium difficile* infection due to a new hypervirulent strain, polymerase chain
- 853 reaction ribotype 078. Clin Infect Dis. 2008;47(9):1162-70. doi: 10.1086/592257. PubMed
- 854 PMID: 18808358.
- 855 31. Lim SC, Knight DR, Riley TV. Clostridium difficile and One Health. Clin Microbiol
- 856 Infect. 2020;26(7):857-63. Epub 20191101. doi: 10.1016/j.cmi.2019.10.023. PubMed PMID:
- 857 31682985.
- 858 32. Bolton D, Marcos P. The Environment, Farm Animals and Foods as Sources of
- 859 Clostridioides difficile Infection in Humans. Foods. 2023:12(5). Epub 20230304. doi:
- 860 10.3390/foods12051094. PubMed PMID: 36900611; PubMed Central PMCID:
- 861 PMCPMC10000743.
- 33. Garrett EM, Sekulovic O, Wetzel D, Jones JB, Edwards AN, Vargas-Cuebas G, et al.
- 863 Phase variation of a signal transduction system controls *Clostridioides difficile* colony
- 864 morphology, motility, and virulence. PLoS Biol. 2019;17(10):e3000379. Epub 20191028. doi:
- 865 10.1371/journal.pbio.3000379. PubMed PMID: 31658249; PubMed Central PMCID:
- 866 PMCPMC6837544.
- 867 34. Thanissery R, Winston JA, Theriot CM. Inhibition of spore germination, growth, and
- 868 toxin activity of clinically relevant C. difficile strains by gut microbiota derived secondary bile
- acids. Anaerobe. 2017;45:86-100. Epub 20170306. doi: 10.1016/j.anaerobe.2017.03.004.
- PubMed PMID: 28279860; PubMed Central PMCID: PMCPMC5466893.
- 871 35. Beebe MA, Paredes-Sabja D, Kociolek LK, Rodriguez C, Sorg JA. Phenotypic analysis
- 872 of various *Clostridioides difficile* ribotypes reveals consistency among core processes. bioRxiv.
- 873 2025. Epub 20250110. doi: 10.1101/2025.01.10.632434. PubMed PMID: 39829883; PubMed
- 874 Central PMCID: PMCPMC11741275.

- 875 36. Ackermann M. A functional perspective on phenotypic heterogeneity in microorganisms.
- Nat Rev Microbiol. 2015;13(8):497-508. Epub 20150706. doi: 10.1038/nrmicro3491. PubMed
- 877 PMID: 26145732.
- 878 37. Aldridge BB, Fernandez-Suarez M, Heller D, Ambravaneswaran V, Irimia D, Toner M,
- et al. Asymmetry and aging of mycobacterial cells lead to variable growth and antibiotic
- susceptibility. Science. 2012;335(6064):100-4. Epub 20111215. doi: 10.1126/science.1216166.
- PubMed PMID: 22174129; PubMed Central PMCID: PMCPMC3397429.
- 882 38. Anjuwon-Foster BR, Tamayo R. A genetic switch controls the production of flagella and
- toxins in *Clostridium difficile*. PLoS Genet. 2017;13(3):e1006701. Epub 20170327. doi:
- 884 10.1371/journal.pgen.1006701. PubMed PMID: 28346491; PubMed Central PMCID:
- 885 PMCPMC5386303.
- 886 39. Anjuwon-Foster BR, Tamayo R. Phase variation of *Clostridium difficile* virulence factors.
- 887 Gut microbes. 2018;9(1):76-83. Epub 20170921. doi: 10.1080/19490976.2017.1362526.
- PubMed PMID: 28806147; PubMed Central PMCID: PMCPMC5914908.
- 889 40. Kint N, Janoir C, Monot M, Hoys S, Soutourina O, Dupuy B, et al. The alternative sigma
- factor sigma(B) plays a crucial role in adaptive strategies of *Clostridium difficile* during gut
- 891 infection. Environ Microbiol. 2017;19(5):1933-58. Epub 20170321. doi: 10.1111/1462-
- 892 2920.13696. PubMed PMID: 28198085.
- 893 41. Courson DS, Pokhrel A, Scott C, Madrill M, Rinehold AJ, Tamayo R, et al. Single cell
- analysis of nutrient regulation of *Clostridioides* (*Clostridium*) difficile motility. Anaerobe.
- 895 2019;59:205-11. Epub 20190803. doi: 10.1016/j.anaerobe.2019.102080. PubMed PMID:
- 896 31386902; PubMed Central PMCID: PMCPMC6785396.
- 897 42. de Jong IG, Beilharz K, Kuipers OP, Veening JW. Live Cell Imaging of Bacillus subtilis
- and Streptococcus pneumoniae using Automated Time-lapse Microscopy. J Vis Exp. 2011;(53).
- 899 Epub 20110728. doi: 10.3791/3145. PubMed PMID: 21841760; PubMed Central PMCID:
- 900 PMCPMC3197447.
- 901 43. Lugagne JB, Lin H, Dunlop MJ. DeLTA: Automated cell segmentation, tracking, and
- lineage reconstruction using deep learning. PLoS Comput Biol. 2020;16(4):e1007673. Epub
- 903 20200413. doi: 10.1371/journal.pcbi.1007673. PubMed PMID: 32282792; PubMed Central
- 904 PMCID: PMCPMC7153852.
- 905 44. O'Connor OM, Alnahhas RN, Lugagne JB, Dunlop MJ. DeLTA 2.0: A deep learning
- pipeline for quantifying single-cell spatial and temporal dynamics. PLoS Comput Biol.
- 907 2022;18(1):e1009797. Epub 20220118. doi: 10.1371/journal.pcbi.1009797. PubMed PMID:
- 908 35041653; PubMed Central PMCID: PMCPMC8797229.
- 909 45. Pogliano J, Osborne N, Sharp MD, Abanes-De Mello A, Perez A, Sun YL, et al. A vital
- 910 stain for studying membrane dynamics in bacteria: a novel mechanism controlling septation
- during *Bacillus subtilis* sporulation. Mol Microbiol. 1999;31(4):1149-59. PubMed PMID:
- 912 10096082; PubMed Central PMCID: PMC2885269.
- 913 46. Garrett EM, Mehra A, Sekulovic O, Tamayo R. Multiple Regulatory Mechanisms
- Ontrol the Production of CmrRST, an Atypical Signal Transduction System in *Clostridioides*
- 915 *difficile*. mBio. 2021;13(1):e0296921. Epub 20220215. doi: 10.1128/mbio.02969-21. PubMed
- 916 PMID: 35164558; PubMed Central PMCID: PMCPMC8844915.
- 917 47. Karasawa T, Ikoma S, Yamakawa K, Nakamura S. A defined growth medium for
- 918 Clostridium difficile. Microbiology (Reading). 1995:141 ( Pt 2):371-5. doi: 10.1099/13500872-
- 919 141-2-371. PubMed PMID: 7704267.

- 920 48. Sauls JT, Cox SE, Do Q, Castillo V, Ghulam-Jelani Z, Jun S. Control of *Bacillus subtilis*
- Replication Initiation during Physiological Transitions and Perturbations. mBio. 2019;10(6).
- 922 Epub 20191217. doi: 10.1128/mBio.02205-19. PubMed PMID: 31848269; PubMed Central
- 923 PMCID: PMCPMC6918070.
- 924 49. Eswaramoorthy P, Duan D, Dinh J, Dravis A, Devi SN, Fujita M. The threshold level of
- the sensor histidine kinase KinA governs entry into sporulation in *Bacillus subtilis*. J Bacteriol.
- 926 2010;192(15):3870-82. Epub 20100528. doi: 10.1128/JB.00466-10. PubMed PMID: 20511506;
- 927 PubMed Central PMCID: PMCPMC2916370.
- 928 50. Narula J, Kuchina A, Zhang F, Fujita M, Suel GM, Igoshin OA. Slowdown of growth
- 929 controls cellular differentiation. Mol Syst Biol. 2016;12(5):871. Epub 20160523. doi:
- 930 10.15252/msb.20156691. PubMed PMID: 27216630; PubMed Central PMCID:
- 931 PMCPMC5289222.
- 932 51. Mehdizadeh Gohari I, Edwards AN, McBride SM, McClane BA. The impact of orphan
- 933 histidine kinases and phosphotransfer proteins on the regulation of clostridial sporulation
- 934 initiation. mBio. 2024;15(4):e0224823. Epub 20240313. doi: 10.1128/mbio.02248-23. PubMed
- 935 PMID: 38477571; PubMed Central PMCID: PMCPMC11210211.
- 936 52. Deatherage DE, Traverse CC, Wolf LN, Barrick JE. Detecting rare structural variation in
- evolving microbial populations from new sequence junctions using breseq. Front Genet.
- 938 2014;5:468. Epub 20150121. doi: 10.3389/fgene.2014.00468. PubMed PMID: 25653667;
- 939 PubMed Central PMCID: PMCPMC4301190.
- 940 53. He M, Sebaihia M, Lawley T, Stabler R, Dawson L, Martin M, et al. Evolutionary
- 941 dynamics of *Clostridium difficile* over short and long time scales. Proceedings of the National
- Academy of Sciences of the United States of America. 2010;107(16):7527-32. doi:
- 943 10.1073/pnas.0914322107.
- 944 54. Sekulovic O, Mathias Garrett E, Bourgeois J, Tamayo R, Shen A, Camilli A. Genome-
- 945 wide detection of conservative site-specific recombination in bacteria. PLoS Genet.
- 946 2018;14(4):e1007332. Epub 20180405. doi: 10.1371/journal.pgen.1007332. PubMed PMID:
- 947 29621238; PubMed Central PMCID: PMCPMC5903667.
- 948 55. Purcell EB, McKee RW, Bordeleau E, Burrus V, Tamayo R. Regulation of Type IV Pili
- 949 Contributes to Surface Behaviors of Historical and Epidemic Strains of *Clostridium difficile*. J
- 950 Bacteriol. 2016;198(3):565-77. Epub 20151123. doi: 10.1128/JB.00816-15. PubMed PMID:
- 951 26598364; PubMed Central PMCID: PMCPMC4719444.
- 952 56. Glomski IJ, Piris-Gimenez A, Huerre M, Mock M, Goossens PL. Primary involvement of
- pharynx and peyer's patch in inhalational and intestinal anthrax. PLoS Pathog. 2007;3(6):e76. doi:
- 954 10.1371/journal.ppat.0030076. PubMed PMID: 17542645; PubMed Central PMCID:
- 955 PMCPMC1885272.
- 956 57. McKenney PT, Yan J, Vaubourgeix J, Becattini S, Lampen N, Motzer A, et al. Intestinal
- 957 Bile Acids Induce a Morphotype Switch in Vancomycin-Resistant Enterococcus that Facilitates
- 958 Intestinal Colonization. Cell Host Microbe. 2019;25(5):695-705 e5. Epub 20190425. doi:
- 959 10.1016/j.chom.2019.03.008. PubMed PMID: 31031170; PubMed Central PMCID:
- 960 PMCPMC6939634.
- 961 58. Leslie JL, Jenior ML, Vendrov KC, Standke AK, Barron MR, O'Brien TJ, et al.
- 962 Protection from Lethal *Clostridioides difficile* Infection via Intraspecies Competition for
- 963 Cogerminant. mBio. 2021;12(2). Epub 20210330. doi: 10.1128/mBio.00522-21. PubMed PMID:
- 964 33785619; PubMed Central PMCID: PMCPMC8092246.

- 965 59. Theriot CM, Koumpouras CC, Carlson PE, Bergin, II, Aronoff DM, Young VB.
- 966 Cefoperazone-treated mice as an experimental platform to assess differential virulence of
- 967 Clostridium difficile strains. Gut microbes. 2011;2(6):326-34. Epub 20111101. doi:
- 968 10.4161/gmic.19142. PubMed PMID: 22198617; PubMed Central PMCID: PMCPMC3337121.
- 969 60. Sachsenheimer FE, Yang I, Zimmermann O, Wrede C, Muller LV, Gunka K, et al.
- 970 Genomic and phenotypic diversity of *Clostridium difficile* during long-term sequential
- 971 recurrences of infection. Int J Med Microbiol. 2018;308(3):364-77. Epub 20180221. doi:
- 972 10.1016/j.ijmm.2018.02.002. PubMed PMID: 29490877.
- 973 61. Semenyuk EG, Poroyko VA, Johnston PF, Jones SE, Knight KL, Gerding DN, et al.
- 974 Analysis of Bacterial Communities during *Clostridium difficile* Infection in the Mouse. Infect
- 975 Immun. 2015;83(11):4383-91. Epub 20150831. doi: 10.1128/IAI.00145-15. PubMed PMID:
- 976 26324536; PubMed Central PMCID: PMCPMC4598419.
- 977 62. Smith AB, Jenior ML, Keenan O, Hart JL, Specker J, Abbas A, et al. Enterococci
- 978 enhance *Clostridioides difficile* pathogenesis. Nature. 2022;611(7937):780-6. Epub 20221116.
- 979 doi: 10.1038/s41586-022-05438-x. PubMed PMID: 36385534; PubMed Central PMCID:
- 980 PMCPMC9691601.
- 981 63. Kim HY, Cho A, Kim JW, Kim H, Kim B. High prevalence of *Clostridium difficile* PCR
- 982 ribotype 078 in pigs in Korea. Anaerobe. 2018;51:42-6. Epub 20180328. doi:
- 983 10.1016/j.anaerobe.2018.03.012. PubMed PMID: 29604338.
- 984 64. Moono P, Foster NF, Hampson DJ, Knight DR, Bloomfield LE, Riley TV. Clostridium
- 985 difficile Infection in Production Animals and Avian Species: A Review. Foodborne Pathog Dis.
- 986 2016;13(12):647-55. Epub 20160907. doi: 10.1089/fpd.2016.2181. PubMed PMID: 27602596.
- 987 65. Burt SA, Siemeling L, Kuijper EJ, Lipman LJ. Vermin on pig farms are vectors for
- 988 Clostridium difficile PCR ribotypes 078 and 045. Vet Microbiol. 2012;160(1-2):256-8. Epub
- 989 20120518. doi: 10.1016/j.vetmic.2012.05.014. PubMed PMID: 22682200.
- 990 66. Dhungel BA, Govind R. Phase-variable expression of pdcB, a phosphodiesterase,
- influences sporulation in *Clostridioides difficile*. Mol Microbiol. 2021;116(5):1347-60. Epub
- 992 20211018. doi: 10.1111/mmi.14828. PubMed PMID: 34606654; PubMed Central PMCID:
- 993 PMCPMC8876291.
- 994 67. Edwards AN, Willams CL, Pareek N, McBride SM, Tamayo R. c-di-GMP Inhibits Early
- 995 Sporulation in *Clostridioides difficile*. mSphere. 2021;6(6):e0091921. Epub 20211208. doi:
- 996 10.1128/msphere.00919-21. PubMed PMID: 34878288; PubMed Central PMCID:
- 997 PMCPMC8653836.
- 998 68. Du S, Henke W, Pichoff S, Lutkenhaus J. How FtsEX localizes to the Z ring and interacts
- with FtsA to regulate cell division. Mol Microbiol. 2019;112(3):881-95. Epub 20190620. doi:
- 1000 10.1111/mmi.14324. PubMed PMID: 31175681; PubMed Central PMCID: PMCPMC6831102.
- 1001 69. Li J, Xu X, Shi J, Hermoso JA, Sham LT, Luo M. Regulation of the cell division
- hydrolase RipC by the FtsEX system in *Mycobacterium tuberculosis*. Nature communications.
- 2023;14(1):7999. Epub 20231204. doi: 10.1038/s41467-023-43770-6. PubMed PMID: 38044344;
- 1004 PubMed Central PMCID: PMCPMC10694151.
- 1005 70. Pichoff S, Du S, Lutkenhaus J. Roles of FtsEX in cell division. Res Microbiol.
- 1006 2019;170(8):374-80. Epub 20190801. doi: 10.1016/j.resmic.2019.07.003. PubMed PMID:
- 1007 31376483; PubMed Central PMCID: PMCPMC6899183.
- 1008 71. Xu X, Li J, Chua WZ, Pages MA, Shi J, Hermoso JA, et al. Mechanistic insights into the
- regulation of cell wall hydrolysis by FtsEX and EnvC at the bacterial division site. Proc Natl

- 1010 Acad Sci U S A. 2023;120(21):e2301897120. Epub 20230515. doi: 10.1073/pnas.2301897120.
- 1011 PubMed PMID: 37186861; PubMed Central PMCID: PMCPMC10214136.
- 1012 72. Garcia-Garcia T, Poncet S, Cuenot E, Douche T, Giai Gianetto Q, Peltier J, et al. Ser/Thr
- 1013 Kinase-Dependent Phosphorylation of the Peptidoglycan Hydrolase CwlA Controls Its Export
- and Modulates Cell Division in *Clostridioides difficile*. mBio. 2021;12(3). Epub 20210518. doi:
- 1015 10.1128/mBio.00519-21. PubMed PMID: 34006648; PubMed Central PMCID:
- 1016 PMCPMC8262956.
- 1017 73. Ransom EM, Williams KB, Weiss DS, Ellermeier CD. Identification and characterization
- of a gene cluster required for proper rod shape, cell division, and pathogenesis in *Clostridium*
- 1019 difficile. J Bacteriol. 2014;196(12):2290-300. doi: 10.1128/JB.00038-14. PubMed PMID:
- 1020 24727226; PubMed Central PMCID: PMC4054185.
- 1021 74. Streett H, Charubin K, Papoutsakis ET. Anaerobic fluorescent reporters for cell
- identification, microbial cell biology and high-throughput screening of microbiota and genomic
- libraries. Curr Opin Biotechnol. 2021;71:151-63. Epub 20210807. doi:
- 1024 10.1016/j.copbio.2021.07.005. PubMed PMID: 34375813.
- 1025 75. Anjou C, Lotoux A, Zhukova A, Royer M, Caulat LC, Capuzzo E, et al. The multiplicity
- of thioredoxin systems meets the specific lifestyles of Clostridia. PLoS Pathog.
- 1027 2024;20(2):e1012001. Epub 20240208. doi: 10.1371/journal.ppat.1012001. PubMed PMID:
- 1028 38330058; PubMed Central PMCID: PMCPMC10880999.
- 1029 76. Shen A, Fimlaid KA, Pishdadian K. Inducing and Quantifying Clostridium difficile Spore
- 1030 Formation. Methods Mol Biol. 2016;1476:129-42. doi: 10.1007/978-1-4939-6361-4\_10. PubMed
- 1031 PMID: 27507338.
- 1032 77. Ransom EM, Weiss DS, Ellermeier CD. Use of mCherryOpt Fluorescent Protein in
- 1033 Clostridium difficile. Methods Mol Biol. 2016;1476:53-67. Epub 2016/08/11. doi: 10.1007/978-
- 1034 1-4939-6361-4 5. PubMed PMID: 27507333.
- 1035 78. Pishdadian K, Fimlaid KA, Shen A. SpoIIID-mediated regulation of sigma(K) function
- during Clostridium difficile sporulation. Mol Microbiol. 2015;95(2):189-208. doi:
- 1037 10.1111/mmi.12856. PubMed PMID: 25393584.
- 1038 79. Fimlaid KA, Jensen O, Donnelly ML, Francis MB, Sorg JA, Shen A. Identification of a
- Novel Lipoprotein Regulator of *Clostridium difficile* Spore Germination. PLoS Pathogens. 2015.
- 1040 Epub October 23, 2015. doi: 10.1371/journal.ppat.1005239.
- 1041 80. Prjibelski A, Antipov D, Meleshko D, Lapidus A, Korobeynikov A. Using SPAdes De
- Novo Assembler. Current protocols in bioinformatics / editoral board, Andreas D Baxevanis [et
- 1043 al]. 2020;70(1):e102. doi: 10.1002/cpbi.102. PubMed PMID: 32559359.
- 1044 81. Seemann T. Prokka: rapid prokaryotic genome annotation. Bioinformatics.
- 1045 2014;30(14):2068-9. Epub 20140318. doi: 10.1093/bioinformatics/btu153. PubMed PMID:
- 1046 24642063.
- 1047 82. Benedict MN, Henriksen JR, Metcalf WW, Whitaker RJ, Price ND. ITEP: an integrated
- toolkit for exploration of microbial pan-genomes. BMC Genomics. 2014;15:8. Epub 20140103.
- 1049 doi: 10.1186/1471-2164-15-8. PubMed PMID: 24387194; PubMed Central PMCID:
- 1050 PMCPMC3890548.
- 1051 83. Eren AM, Kiefl E, Shaiber A, Veseli I, Miller SE, Schechter MS, et al. Community-led,
- integrated, reproducible multi-omics with anvi'o. Nat Microbiol. 2021;6(1):3-6. doi:
- 10.1038/s41564-020-00834-3. PubMed PMID: 33349678; PubMed Central PMCID:
- 1054 PMCPMC8116326.

- 1055 84. van Dongen S, Abreu-Goodger C. Using MCL to extract clusters from networks.
- 1056 Methods Mol Biol. 2012;804:281-95. doi: 10.1007/978-1-61779-361-5 15. PubMed PMID:
- 1057 22144159.
- 1058 85. Deatherage DE, Barrick JE. Identification of mutations in laboratory-evolved microbes
- from next-generation sequencing data using breseq. Methods Mol Biol. 2014;1151:165-88. doi:
- 1060 10.1007/978-1-4939-0554-6\_12. PubMed PMID: 24838886; PubMed Central PMCID:
- 1061 PMCPMC4239701.
- 1062 86. César N. Dataset for the article: Unique growth and morphology properties of Clade 5
- 1063 Clostridioides difficile strains revealed by single-cell time-lapse microscopy. Zenodo. 2024. doi:
- 1064 https://doi.org/10.5281/zenodo.13352469.
- 1065 87. Sebaihia M, Wren B, Mullany P, Fairweather N, Minton N, Stabler R, et al. The
- multidrug-resistant human pathogen *Clostridium difficile* has a highly mobile, mosaic genome.
- 1067 Nature genetics. 2006;38(7):779-86. doi: 10.1038/ng1830.
- 1068 88. Stabler R, He M, Dawson L, Martin M, Valiente E, Corton C, et al. Comparative genome
- and phenotypic analysis of *Clostridium difficile* 027 strains provides insight into the evolution of
- 1070 a hypervirulent bacterium. Genome biology. 2009;10(9). doi: 10.1186/gb-2009-10-9-r102.
- 1071 89. Kurka H, Ehrenreich A, Ludwig W, Monot M, Rupnik M, Barbut F, et al. Sequence
- similarity of *Clostridium difficile* strains by analysis of conserved genes and genome content is
- reflected by their ribotype affiliation. PLoS One. 2014;9(1):e86535. Epub 20140123. doi:
- 1074 10.1371/journal.pone.0086535. PubMed PMID: 24482682; PubMed Central PMCID:
- 1075 PMCPMC3902958.
- 1076 90. Moura I, Monot M, Tani C, Spigaglia P, Barbanti F, Norais N, et al. Multidisciplinary
- analysis of a nontoxigenic *Clostridium difficile* strain with stable resistance to metronidazole.
- Antimicrobial agents and chemotherapy. 2014;58(8):4957-60. Epub 20140609. doi:
- 1079 10.1128/AAC.02350-14. PubMed PMID: 24913157; PubMed Central PMCID:
- 1080 PMCPMC4135993.
- 1081 91. Thorpe CM, McDermott LA, Tran MK, Chang J, Jenkins SG, Goldstein EJC, et al. U.S.-
- Based National Surveillance for Fidaxomicin Susceptibility of Clostridioides difficile-Associated
- Diarrheal Isolates from 2013 to 2016. Antimicrobial agents and chemotherapy. 2019;63(7). Epub
- 1084 20190624. doi: 10.1128/AAC.00391-19. PubMed PMID: 31085514; PubMed Central PMCID:
- 1085 PMCPMC6591623.

1089 1090

1091

1092

1093

1094

1095

1096

1097

1098

1099

1100

1101

1102

1103

1104

1105

1106

1107

1108

1109

1110

1111

1112

1113

1114

1115

1116

1117

1118

1119

**Figure Legends Figure 1. Schematic of the anaerobic single-cell imaging set-up.** Exponentially growing C. difficile cells in TY medium supplemented with cysteine (TYC) are spotted onto 1.5% agarose pads formed within gas-tight adhesive Gene Frames inside the anaerobic chamber. Up to 6 strains can be spotted onto a pad. The pad is sealed with a coverslip, and the imaging chamber is removed from the anaerobic chamber and transferred to a heated (37°C) microscope stage. Time-lapse microscopy is used to visualize the growth of individual bacterial cells for 2-6 hrs. The output data is segmented and tracked with the DeLTA Python package (191). An example filmstrip of strain 630 grown on TYC medium over time is shown (Bottom). Figure 2. Clade 5 strain M120 elongates more quickly and exhibits cell chaining. (A) Violin plot of the elongation rates measured during time-lapse microscopy analyses of strains 630 (Clade 1), R20291 (Clade 2), E15 (Clade 3), M68 (Clade 4), and M120 (Clade 5) grown on TY supplemented with cysteine (TYC) agar. Data are from three biological replicates, with the mean of each replicate shown as a point on the violin. (B) Optical density-based analyses of bulk population growth of the indicated strains in TYC or BHIS media. The number in brackets indicates the clade to which a given strain belongs. (C) Violin plot of the cell or chain length measured during time-lapse microscopy for the strains shown in A. Each replicate mean is shown as a point on the violin. Statistical significance for A and B was determined by comparing the mean of the three replicates of strains from Clades 1-4 strains relative to the Clade 5 M120 strain using a Kruskal-Wallis test \* p < 0.05. (B) Phase-contrast image from time-lapse microscopy movies. Scale bar is 10 µm. Figure 3. C. difficile Clade 5 can form large heterogenous chains. Large mosaic phasecontrast image of the Clade 5 strain M120. Inset shows chains revealed by staining with the membrane dye FM4-64; septa are highlighted with yellow arrows. The image was stitched from 8 individual fields of view at 63X magnification. Scale bar is 100 µm. Figure 4. Faster growth is a common feature of Clade 5 strains, but the chaining phenotype is not fully penetrant in Clade 5 strains. (A) Phase-contrast microscopy images from time-lapse microscopy studies of Clade 5 strains; Clade 1 strain 630 is included for

1121

1122

1123

1124

1125

1126

1127

1128

1129

1130

1131

1132

1133

1134

1135

1136

1137

1138

1139

1140

1141

1142

1143

1144

1145

1146

1147

1148

1149

1150

comparison. Fluorescence microscopy was used to visualize the FM4-64 stain incorporated into the agarose pads. Masks generated using DeLTA are shown, with the bottom panel showing division septa identified with our adaptive thresholding approach (red dots). (B) Example image showing the parameters identified using DeLTA combined with our adaptive threshold method for detecting division septa (red dot) within a chain of cells. Following the automated thresholding analysis for detecting septa, the images were manually inspected to ensure that all septa were properly identified. (C) Cell or chain length measured using automated DeLTA analyses (pink violin plot) or DeLTA combined with the adaptive threshold-manual inspection analyses (purple violin plot). The former method is more likely to measure chain length, while the latter method accurately measures cell length. (D) Violin plot of the elongation rates measured based on three biological replicates. Each replicate mean is shown as a point on the violin; statistical significance was determined by comparing the mean of the three replicates using a Kruskal-Wallis test, \* p < 0.05. Figure 5. Clade 5 strains form chains during logarithmic growth in broth culture. Representative micrographs showing phase-contrast (top) and peptidoglycan labeling with the fluorescent D-amino acid, HADA, (bottom) following growth in rich broth (BHIS) to midlogarithmic phase. All strains shown, with the exception of Clade 1 strain 630, are Clade 5 strains. Scale bar, 10 µm. Data are representative of three independent experiments. ADJ indicates that the brightness of the image was enhanced to detect HADA labeling in V48. Figure 6. Sporulation levels in Clade 5 isolates grown on 70:30 medium. Phase-contrast microscopy of the indicated strains ~24 hrs after sporulation induction. All strains shown with the exception of 630 (Clade 1) are Clade 5 strains. The percent heat-resistant spores is indicated below the respective images. The percentage was determined from 20-24 hr sporulating cultures and represent the mean and standard deviation for a given strain based on a minimum of three biological replicates. Statistical significance relative to strain 630 was determined using a oneway ANOVA and Tukey's test. The scale bar represents 5 µm. Figure 7. The orientation of the *cmr* switch promotes Clade 5 strain cell chaining and surface motility. (A) Orientation-specific qPCR for detecting the orientation of the cmr switch

1152

1153

1154

1155

1156

1157

1158

1159

1160

1161

1162

1163

1164

1165

1166

1167

1168

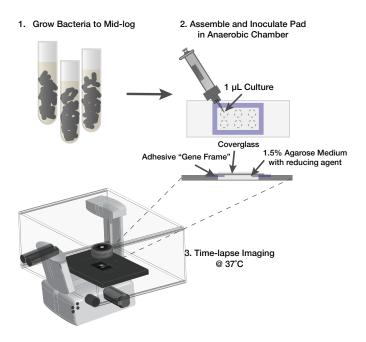
1169

1170

1171 1172

in the indicated strains. The mean and standard deviation based on one to three biological replicates are shown. Statistical significance relative to strain TAL29996 was determined using a one-way ANOVA and Tukey's test for strains where data from three independent experiments was obtained. \*\*\*\* p < 0.0001. (B) Representative micrographs of cmrRST CRISPRi knockdown strains compared to a no target control. Phase-contrast (top) and peptidoglycan labeling with the fluorescent D-amino acid, HADA, (bottom) images following growth in rich broth (BHIS) to mid-logarithmic phase. Scale bar, 5 μm. (C) Representative images of surface motility 5 days after exponentially growing liquid cultures of the indicated strains were spotted onto BHIS agar plates. Figure 8. Infection and colonization dynamics of Clade 5 strains in mice. (A) Fecal colonyforming units measured by selective plating and (B) Percentage of weight loss to baseline of infected mice on Days 1-4, 7, and 14. The mean and standard deviation are shown based on the results of two experiments consisting of four mice each (n = 8). (C) Percentage of *cmr*-ON switch orientation measured in fecal pellets on the indicated days by qPCR. For the strain TAL29996 inoculum, 1% of the spores had the *cmr*-ON switch orientation, while the TAL29600 inoculum consisted of 32% cmr-ON spores. The mean and standard deviation based on analyses of eight mice are shown, although fecal pellets could not be collected from some of the mice on Day 2. The same mouse exhibited a higher *cmr*-ON frequency for TAL29600 over time (15%, Day 7 and 27%, Day 14).

**Supporting Information** S1 Fig. Growth rates measured from optical density-based analyses of bulk population growth in TYC and BHIS media. S2 Fig. Optical density-based analyses of bulk population growth of the indicated strains during growth in TYC and BHIS media. S3 Fig. Clade 5, but not Clade 1 or 4, strains form chains during logarithmic growth in BHIS broth culture. S4 Fig. Clade 5 strains form chains even when growth is slowed during growth in minimal medium broth culture. S5 Fig. Sporulation levels in clinical isolates grown on 70:30 medium. S6 Fig. Spores purified from Clade 5 strains. S7 Fig. Expression of the *cmrRST* operon promotes cell chaining. S8 Fig. Cell length during growth on 70:30 sporulation medium. S9 Fig. Surface motility in Clade 1-4 strains. S10 Fig. Infection and cmr switch orientation dynamics during TAL29600 infection. S1 Table. Average nucleotide identity for orthologous genes for Clade 5 strains S2 Table. Breseq analyses of Clade 5 strain genomes. S3 Table. Anvi'o analysis of the accessory genome identified for the Clade 5 strains sequenced.



4. Cell Segmentation using DeLTA

